Journal of Alloys and Compounds 689 (2016) 439–445

Contents lists available at ScienceDirect

Journal of Alloys and Compounds

journal homepage: http://www.elsevier.com/locate/jalcom

Surface enhanced Raman scattering substrate with high-density hotspots fabricated by depositing Ag film on TiO_2-catalyzed Ag nanoparticles

Shuai Li [a, b, *], Dawei Li [b], Qing-Yu Zhang [b, **], Xin Tang [c]

[a] College of Science, Guilin University of Technology, Guilin, 541004, China
[b] Key Laboratory of Materials Modification by Laser, Ion and Electron Beams, School of Physics & Optoelectronic Technology, Dalian University of Technology, Dalian, 116024, China
[c] College of Material Science and Engineering, Guilin University of Technology, Guilin, 541004, China

ARTICLE INFO

Article history:
Received 27 May 2016
Received in revised form
26 July 2016
Accepted 27 July 2016
Available online 2 August 2016

Keywords:
Ag nanoparticles
Photocatalytic growth
SERS substrate

ABSTRACT

Surface enhanced Raman scattering (SERS) has been developed as a powerful tool for detection of ultra-trace molecules, thus at foundation of a number of important technologies, such as chemical analysis and biosensor. Photocatalytic growth of Ag nanoparticles (NPs) by TiO_2 film is a cost-effective, facile and surfactantless way to fabricate SERS substrates with high stability and reproducibility, but the SERS activity still needs to be improved. In this work, we report a facile way to improve SERS activity of TiO_2-catalyzed Ag NPs by additionally depositing a layer of Ag film using magnetron sputtering. Combining with the advantages of liquid and vapor environment, the Ag NPs size increase to the resonance size without decrease of density, so the spacing of Ag NPs decrease and high-density hotspots can be formed. By optimizing the sputtering time of Ag films, the SERS activity of the Ag NPs/films is improved by a factor of ~400. This work not only establish a low-cost method for fabricating high-quality SERS substrate, more importantly, propose a novel way to prepare plasmonic nanostructures with high-density hotspots.

1. Introduction

Surface enhanced Raman scattering (SERS), which occurs on rough metallic (typically Au and Ag) surfaces or nanoparticles (NPs), has been intensely explored as a highly sensitive technique for detection of ultra-trace or single molecule [1–3]. For the purpose of SERS application in chemical analysis and biosensing, a key step is fabrication of high-quality SERS substrates, which needs to be highly sensitive, reproducible, stable over time, easy to be fabricated, and cost-effective [4]. In the past decades, many methods have been explored to fabricate various nanostructures for SERS substrates, such as cycling oxidation-reduction of Ag electrode surface [5], deposition of metallic island films [6] or Ag nanorods [7], lithography for ordered Ag nanostructures [8,9] or three-dimensional metal nanostructures [10,11]. Though these methods are potential for fabrication of SERS substrate, there is a necessity to be further improved in the viewpoint of practical applications. For example, lithography is capable of fabricating a SERS substrate with highly controlled hotspots, but its high cost is obstructive to commercial application. Extremely high SERS activity was claimed to achieve on Ag-decorated three-dimensional nanostructures [12–14], but the reproducibility needs to be improved. Therefore, it is necessary to explore the way for commercial applications.

Because of the excellent photocatalytic activity, TiO_2 films have been widely used to grow Ag NPs on the surface of TiO_2 films by reducing the Ag^+ in $AgNO_3$ aqueous solution under the irradiation of ultraviolet (UV) light [15–19]. The TiO_2-catalyzed Ag NPs can be used as SERS substrate with the following advantages. First, photocatalytic reduction is a cost-effective method facilitating fabrication of TiO_2-catalyzed Ag NPs, in which the semiconductor (TiO_2) and Ag NPs synergically contribute to Raman enhancement. Second, the TiO_2-catalyzed Ag NPs prepared by the photocatalytic reduction are surfactant free, thus preventing against the contamination in SERS measurement from the agents, which are usually necessary in

* Corresponding author. College of Science, Guilin University of Technology, Guilin, 541004, China.
** Corresponding author.
E-mail addresses: lishuai@glut.edu.cn (S. Li), qyzhang@dlut.edu.cn (Q.-Y. Zhang).

http://dx.doi.org/10.1016/j.jallcom.2016.07.303
0925-8388/

synthesis of noble metallic NPs by other solution-phase reactions, such as the chemical synthesis of Ag NPs in colloids. Third, the TiO_2-catalyzed Ag NPs are stable for long-time use (>1 year) [16]. More importantly, the TiO_2-catalyzed Ag NPs is very uniform in size and controllable, thus leading to a high reproducibility in acquiring Raman signals. For example, Li et al. [17] found the spot-to-spot variance in Raman signals on the TiO_2-catalyzed Ag NPs as small as ~10%, which is a good performance among various SERS substrates. Despite of above advantages, the TiO_2-catalyzed Ag NPs are still absent of enough attention, because the SERS activity needs to be improved when they are used as SERS substrates.

It is well known that the electromagnetic hotspots, which mainly occurred in the nanogaps less than 10 nm, make the most important contribution to the Raman enhancement in SERS substrates [20–23]. By investigations into the TiO_2-catalyzed Ag NPs, the spacing between adjacent Ag NPs was found too large to form hotspot, thus producing a relatively low SERS activity [17]. Systemic study revealed that the liquid environment is a major factor resulting in the wide gaps between the Ag NPs [24]. In the liquid environment, Ostwald ripening is the dominative mechanism controlling the photocatalytic growth of Ag NPs, as schematically shown in Fig. 1(a), and then leading to a wide distribution of Ag NPs in size, as shown in Fig. 1(c), and a lower density, thus obstructing the formation of high-density hotspots. This shortage cannot be overcome in the photocatalytic growth of TiO_2-catalyzed Ag NPs. Therefore, we have to explore other methods for improving the SERS activity of the TiO_2-catalyzed Ag NPs.

Differing from the photocatalytic growth of Ag NPs in liquid environment, OR-dominated growth of Ag NPs is limited at room temperature in physical vapor deposition (PVD), such as magnetron sputtering. After nucleation, the Ag NPs deposited by magnetron sputtering could uniformly grow up without obvious OR process, as schematically shown in Fig. 1(a) and the SEM image in Fig. 1(d). High-density hotspots have been obtained in deposition of Ag films at the percolation threshold [25], but the sizes of Ag NPs is at a level of 10–30 nm, which is too small to produce a stronger Raman resonance under excitation of visible light. Moreover, there is a difficulty in technology controlling the growth of Ag NPs at the percolation threshold. After the point of percolation threshold, coalescence of Ag NPs will take place, and then resulting in formation of Ag film, which exhibits a rather low SERS activity, as shown in Fig. 1(b).

The different growth modes between vapor and liquid environment make us think of a novel way to fabricate SERS substrates with high-density hotspots by combining the photocatalytic growth and magnetron sputtering. It can be expected that the limited OR growth of Ag NPs in vapor environment will increase the size of TiO_2-catalyzed Ag NPs without decrease its density, leading to the formation of high-density hotspots.

In this work, we report our attempt to fabricate a new SERS substrate with high-density hotspots by depositing a layer of Ag film on the TiO_2-catalyzed Ag NPs using magnetron sputtering method. The enhancement of Raman signals was studied as a function of deposition time of Ag films, and an enhancement factor as large as ~1.2×10^7 was obtained by optimizing the deposition time of Ag films. This method was demonstrated easily to control the SERS activity of TiO_2-catalyzed Ag NPs at a relatively high level, which is comparable with the SERS substrates fabricated by lithography or other methods. In addition, we studied the dependence of hotspots on the deposition time and gave a discussion on the enhancement mechanism in the SERS substrates.

2. Experimental details

2.1. Preparation of TiO_2 films

Nanoparticulate TiO_2 films for depositing Ag NPs were

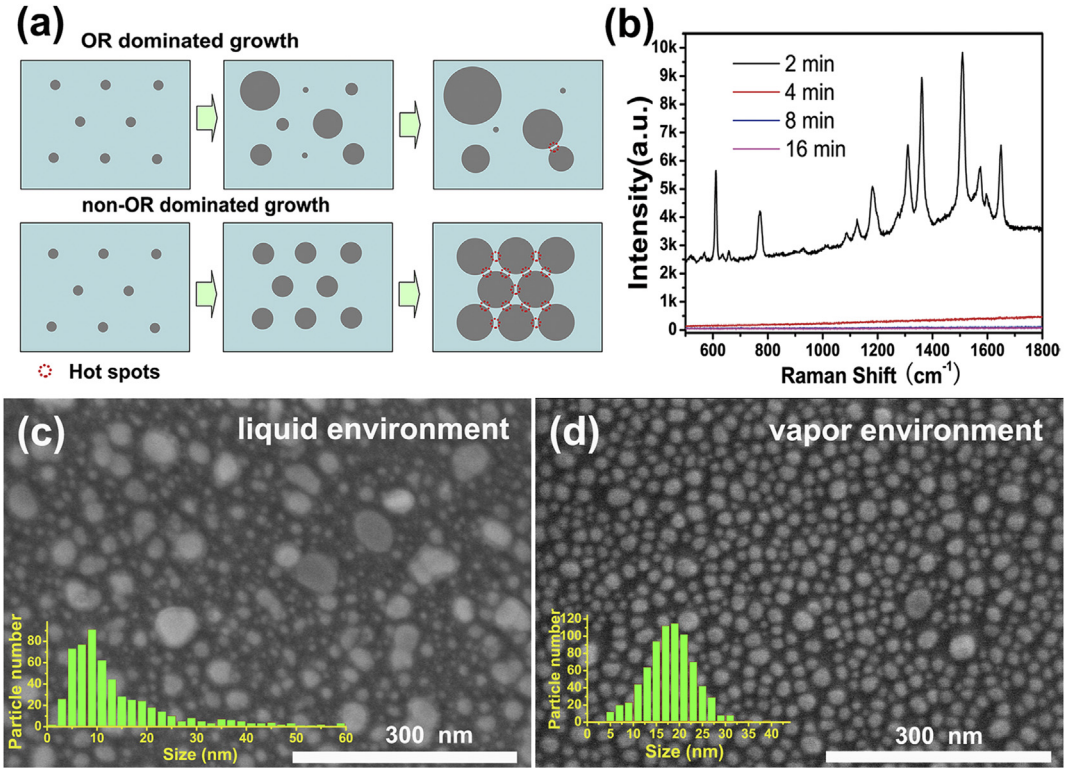

Fig. 1. (a) Schematic diagrams of NP growth in solution and in vacuum. (b) Raman spectra of R6G on Ag films deposited at the given time. (c) SEM image of the typical TiO_2-catalyzed Ag NPs prepared by photocatalytic method. (d) SEM image of the typical Ag NPs prepared by sputtering method.

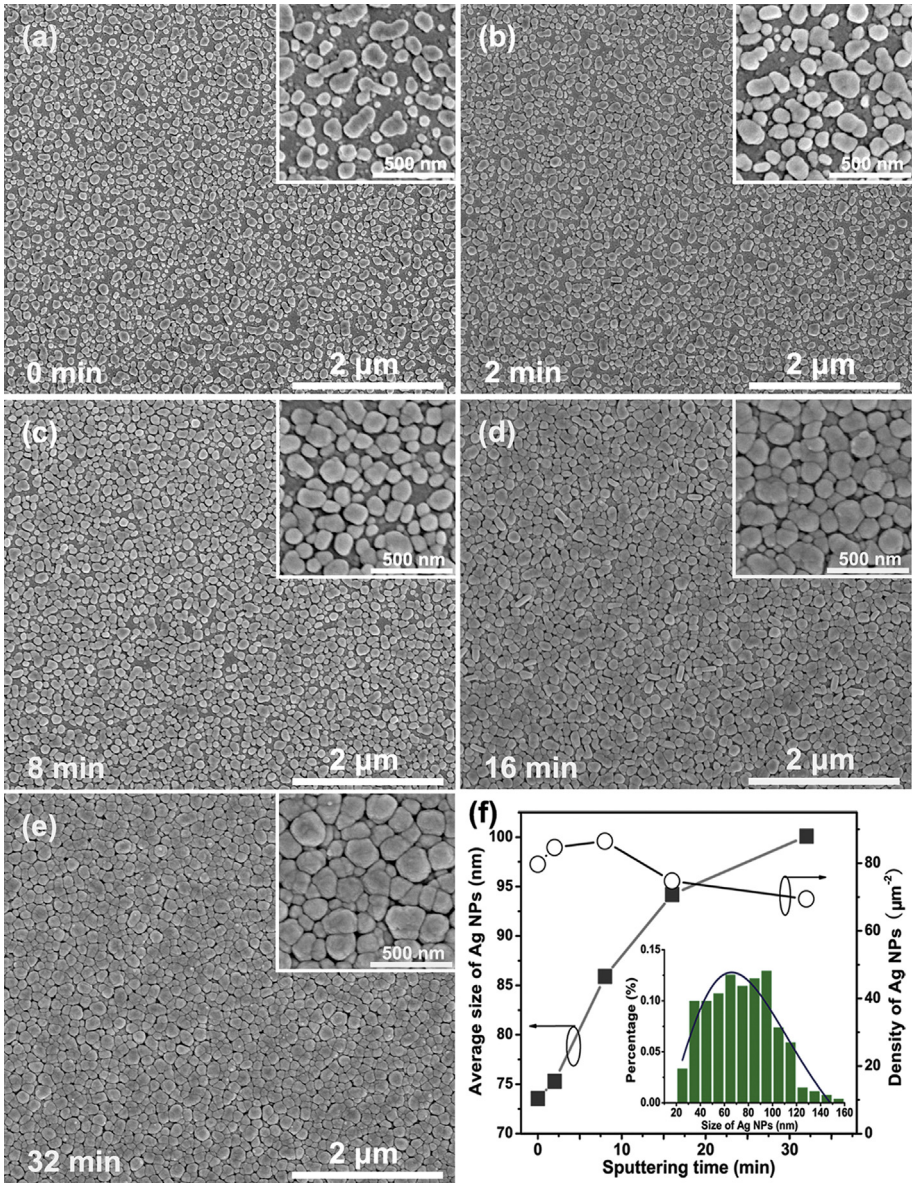

Fig. 2. (a–e) SEM images of Ag–TiO_2 films before and after Ag deposition at the given time, (f) Average size and density of Ag NPs plotted as a function of Ag deposition time. The inset shows the size distributions of the TiO_2-catalyzed Ag NPs before Ag deposition.

prepared by the conventional sol-gel method. Namely, 50 mL titanium isopropoxide was first mixed with 3 mL acetylacetone and stirred about 10 min (solution A). Then, 0.21 mL nitric acid, 1.4 mL deionized water and 150 mL ethyl alcohol were mixed and stirred for ~10 min (solution B). The TiO_2 sol was prepared by slowly adding solution B dropwise into the vigorously stirring solution A. After mixing, the TiO_2 sol was kept stirring for 2 h at room temperature and aged for 2 days for use. TiO_2 gel films were coated on the substrate of cleaned glass slide with dip-coating method by immersing the substrate into the as-prepared TiO_2 sol. At last, the TiO_2 gel film was crystallized at 450 °C for 1 h to form anatase TiO_2 film. The thickness of TiO_2 films was controlled at ~200 nm. To avoid any contamination, the TiO_2 films were immediately used to grow Ag NPs. All the chemicals in the preparation of TiO_2 films were of analytical reagent grade and were purchased from Kermel Chemical Reagents Co. Ltd.

2.2. Growth of Ag NPs and sputtering of Ag films

The growth of Ag NPs was conducted in $AgNO_3$ solution of 180 mg/L (1 mM) under the irradiation of a low-pressure mercury lamp (Philips TUV, Amsterdam, Holland, 8 W). The experimental setup was placed in a dark room. The distance from the lamp to the TiO_2-coated film was fixed at 6 cm and the illumination flux of ultraviolet (UV) photons (>3.1 eV) was estimated to be $10^{16}/cm^2 \cdot s$. The growth process was monitored by *in-situ measurement of* extinction spectra in the wavelength range of 200–1100 nm using ultraviolet–visible-near-infrared spectroscopy (UV–Vis.-NIR, Ocean, Maya 2000-Pro Dunedin FL). After the growth was stopped, the samples were taken out, carefully cleaned, and dried with a slow flow of dry nitrogen. The deposition of Ag films were at room temperature by sputtering a silver target (99.99%) using a magnetron sputtering system operated at 0.5 Pa in an ambient of Ar. To

optimize the SERS activity, the Ag films were deposited on TiO_2–Ag NPs for 2, 4, 8, 16, and 32 min, respectively.

2.3. Characterizations of Ag NPs and Ag NPs/film

Scanning electron microscopy (SEM, Nova NanoSEM 450, FEI) was used to characterize the morphology of TiO_2-catalyzed Ag NPs before and after optimization. The size distribution of Ag NPs and hotspots length in SEM images were studied using the software for statistical analysis. To study the change in extinction, Maya 2000-Pro was used to the transmittance spectra of TiO_2-catalyzed Ag NPs before and after optimization. The SERS measurement was performed on a Raman spectroscopy (Renishaw inVia plus Renishaw) using R6G as molecular probe by dropping a 50 μL of 1 μM R6G aqueous solution on the TiO_2-catalyzed Ag NPs. At the same time, the same volume of 0.01 M R6G aqueous solution on a TiO_2 film was used as a reference to determine the Raman enhancement factor (EF_{SERS}). The EF_{SERS} is experimentally defined as [26].

$$EF_{SERS} = \frac{I_{SERS}/N_{Surf}}{I_{Ref}/N_{Ref}} \quad (1)$$

where I_{SERS} and I_{Ref} are the intensities of Raman signals measured from the SERS and the reference samples, respectively. N_{SERS} and N_{Ref} are the corresponding numbers of R6G molecules within the irradiated areas. The measurement was conducted under the conditions as follows: a 632.8 nm He–Ne laser with a power of 3.28 mW was used as the source of exciting light; a 50 × objective was used to focus the laser beam onto the sample surface and to collect the Raman signals; the size of laser spot was about 2 μm and the spectra were recorded at three positions with an integral time of 10 s.

3. Results and discussion

Fig. 2 (a–e) shows the typical SEM images of TiO_2-catalyzed AgNPs before and after optimization by depositing a layer of Ag film with different deposition time. All the Ag NPs exhibit the similar shapes and uniformly distribute on the TiO_2 surface, but their sizes vary with Ag deposition, as shown in the insets. As shown in Fig 2 (a), most of the as-grown Ag NPs on the TiO_2 surface are in the sizes ranging 40–100 nm, leaving the spacing between two adjacent Ag NPs rather large, thus there are few gaps could be regarded as the electromagnetic hotspots in the SEM image. With Ag deposition, the Ag NPs gradually grow up, and then the spacing among them changes to be narrower and narrower. For the samples with Ag deposition less than 8 min, the Ag NPs are not large enough, and then the hotspots with the spacing less than 10 nm are still rare in the images. For the samples with Ag deposition time of 16 min or 32 min, the Ag NPs have an average size close to 100 nm. As most of Ag NPs are looked in contact, high-density hotspots are expected in these samples. The statistical analysis, as shown in Fig. 2(f), also revealed that the average size of Ag NPs increase from 73 nm to 100 nm with the increase of Ag deposition time while the density of Ag NPs maintain a nearly constant, thus leading to a reduction of the spacing between adjacent Ag NPs and the high-density hotspots.

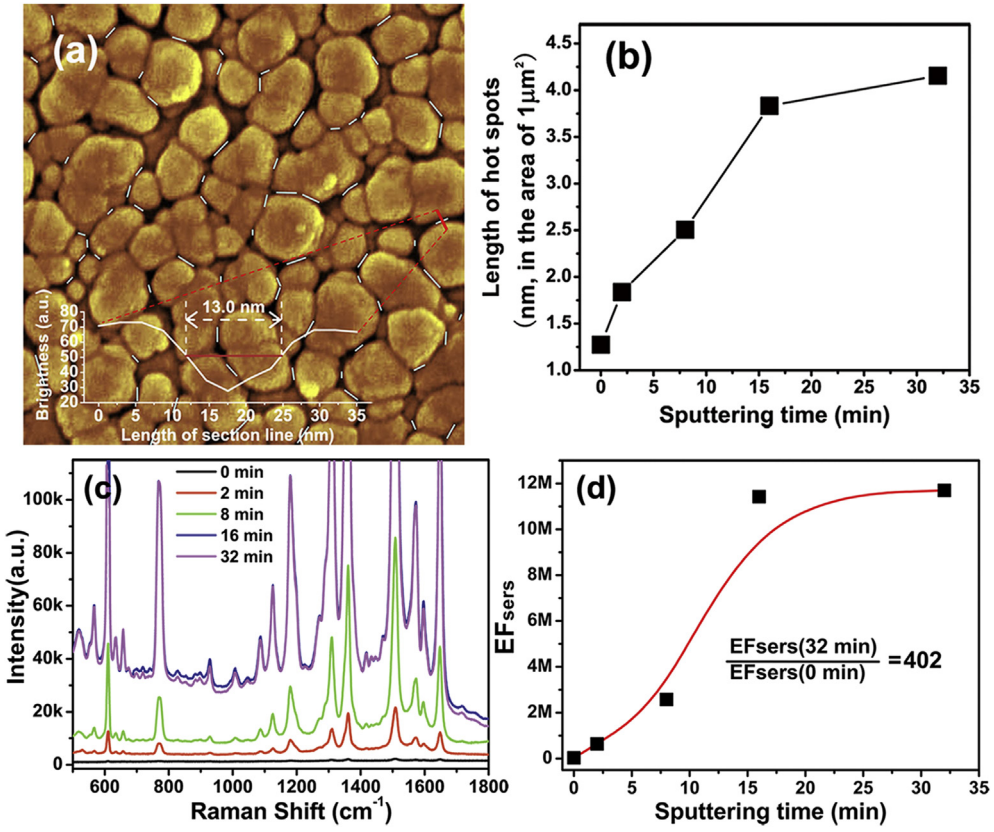

Fig. 3. (a) Topological image of the TiO_2-catalyzed Ag NPs optimized by Ag deposition for 16 min. The inset shows the profile along the red solid line across the gap between two adjacent Ag NPs. (b) Total length of hotspots in a 1 μm^2 area plotted as a function of Ag deposition time. (c) Raman spectra of R6G molecules on the TiO_2-catalyzed Ag NPs before and after Ag deposition at the given time, (d) SERS enhancement of the optimized Ag–TiO_2 films plotted as a function of Ag deposition time. (For interpretation of the references to colour in this figure legend, the reader is referred to the web version of this article.)

To have a deep understanding, we quantitatively calculated the total length of hotspots in a SEM image. The hotspots are defined to be the gaps with a spacing less than 15 nm in this study. Fig. 3(a) shows an example how to determine the hotspot length in gaps. First, we plotted a line (the red solid line) across the gap to obtain a profile, as shown in inset in the figure. Then, the width can be determined by the full width at half maximum (FWHM). Using the FWHM of line profiles, the hotspot length in a gap could be estimated. In Fig. 3(a), the white bars are the determined hotspots using this method. In Fig 3(b), we plot the total length of hotspots per 1 μm^2 SEM image as a function of Ag deposition. With the increase in Ag deposition time, the hotspot length gradually increases from 1.3 to 4.7 nm. At the beginning for Ag deposition, the increase in the hotspot length is almost a linear function of deposition time. For a longer deposition, the increment of the hotspot length changes to be smaller, because coalescence of Ag NPs takes place. This result suggests that the deposition of Ag film is easily to optimize TiO_2-catalytic Ag NPs with a relatively high density of hotspots.

Above conclusions are definitely evidenced by the following SERS measurement. Fig. 3(c) shows the Raman spectra of 1 μM R6G molecules taken from the TiO_2-catalyzed Ag NPs before and after optimization by deposition of Ag films. All the featured bands of R6G molecules are clearly identified in the Raman spectra. The sharp peak at 612 cm^{-1} is associated with the in-plane bending vibration of C—C—C ring, peaks at 770 and 1130 cm^{-1} are assigned to the out-of-plane and in-plane bending vibrations of C—H, respectively. The bands at 1362, 1510, and 1650 cm^{-1} originate from the aromatic stretching vibrations [27]. With the increase in Ag deposition time up to 16 min, the Raman intensities increase, and then maintain a the high levels when the deposition time changes from 16 to 32 min. Using the Raman intensity at 612 cm^{-1} of 0.1 M R6G on a pure TiO_2 film as the reference, the enhancement factors of SERS (EF_{SERS}) are determined by carefully calculating the numbers of R6G molecules in the irradiating area, and then plotted as a function of Ag deposition time, as shown in Fig. 3(d). Before Ag deposition, the EF_{SERS} value of TiO_2-catalytic Ag NPs is at a level of ~3×10^4. Ag deposition by magnetron sputtering produces an increase in EF_{SERS} up to ~1.2×10^7, thus the SERS activity of TiO_2-catalytic Ag NPs is enhanced by a factor of ~400. The optimized SERS activity is good enough for commercial application, whereas the method to fabricate SERS substrates is cost-effective and much easier than others. With the increase in Ag deposition, the EF_{SERS} value exhibits an increasing trend very similar to the hotspot density, indicating that the increase in the hotspots by deposition of Ag films plays a crucial role in improving the SERS activities of TiO_2-catalytic Ag NPs.

Raman mapping was also used to evaluate the SERS improvement of TiO_2-catalyzed Ag NPs by Ag deposition. We prepared a sample in which four different areas are included, namely, an area with pure TiO_2 film (TiO_2), an area with TiO_2 film covered by a layer of Ag film (TiO_2/Ag film), an area with Ag NPs on TiO_2 film (TiO_2/Ag

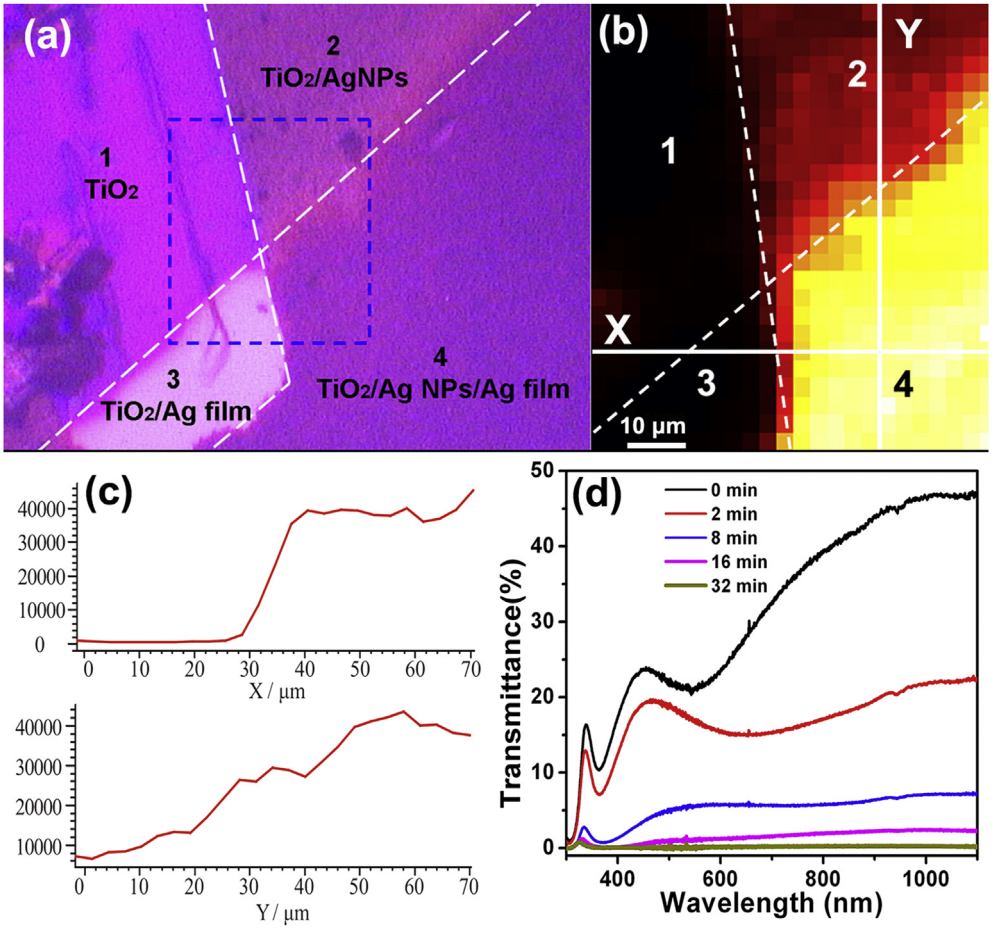

Fig. 4. (a) Optical micrograph of a sample with four different areas, (b) Raman mapping taken from the square region defined by the blue dash lines in Fig. 4(a). (c) Raman intensities at 1508.95 cm^{-1} taken along the x and y directions indicated by the white solid lines in Fig. 4(b). (d) Transmission spectra of the TiO_2-catalyzed Ag NPs before and after Ag deposition at the given time. (For interpretation of the references to colour in this figure legend, the reader is referred to the web version of this article.)

NPs), and an area with TiO_2/Ag NPs optimized by a layer of Ag film (TiO_2/Ag NPs/Ag film). These different areas are numbered as 1, 2, 3, and 4, respectively, as shown in Fig. 4(a), which was an image taken by an optical microscope. Fig. 4(b) shows the SERS mapping taken from the square area (70 μm × 70 μm) defined by the blue dashed lines in Fig. 4(a). The Raman mapping was collected by point-to-point imaging with a step of 3 μm using the Raman peak of R6G at 1508.95 cm^{-1}. The brightness in the image is proportional to the intensity of Raman signal. The difference in SERS activity is obvious in the Raman mapping. As shown in the image, the Raman signals in the area of TiO_2 film are lowest, and additional Ag film cannot make the Raman signals on TiO_2 film obviously enhanced, indicating that the SERS activity in these areas is rather low. The TiO_2-catalyzed Ag NPs produce a considerable Raman enhancement, but the Raman intensity in the area of TiO_2/Ag NPs is still much lower than those in the optimized area by deposition of Ag film, in accordance with our conclusion obtained using the individual SERS substrates. The Raman mapping reveals a fact that the Raman signals on the optimized TiO_2-catalytic Ag NPs have good uniformity and reproducibility, which are important for the purpose of commercial application. Fig. 4(c) shows the quantitative Raman intensities taken along x and y directions indicated by the white solid lines in Fig. 4(b). We can see that the Raman signals are close to 0 in the black area, and as high as ~40000 in the bright yellow area.

We noticed that the area of TiO_2/Ag film is the brightest in the optical micrograph in Fig. 4(a), suggesting the reflectance of Ag film is the largest. However, the TiO_2-catalyzed Ag NPs/Ag film is darker than the TiO_2-catalyzed Ag NPs, indicating that the reflectance decreased after deposition of Ag film. Spectral measurement also revealed that the transmittance of the sample with TiO_2-catalyzed Ag NPs decreases with the increase in Ag deposition time, as shown in Fig. 4(d). Therefore, we have a conclusion that the absorbance of the TiO_2-catalyzed Ag NPs is enhanced after deposition of Ag film, because transmittance + reflectance + absorbance = 1. The enhancement in absorbance can be attributed to the stronger interaction between the incident light and electrons in Ag NPs, or the enhanced plasmonic excitation. This result is different from previous reports for other metallic NPs/film structures [28–30]. In these studies, the reflectance of metallic NPs was increased after depositing a layer of film, and then the improvement in SERS activity was attributed to the enhanced local electromagnetic field associated with superposition of the incident wave and the reflection wave. In this study, we are convinced of that the increase in the hotspot density produces an enhancement in light trapping, thus optimizing the SERS activity of TiO_2-catalytic Ag NPs to be possible in commercial application in future.

4. Conclusions

In summary, we report a facile and cost-effective method to considerably improve the SERS activity of TiO_2-catalyzed Ag NPs by depositing a layer of Ag film. The enhancement factor of optimized SERS substrate could be increased up to 1.2×10^7, which is high enough for practical applications in chemical analysis and biosensoring. The SERS activity is highly uniform and reproducible. More importantly, the SERS activity is easily optimized at a relatively high level by controlling Ag deposition time, thus meeting the requirement for massive fabrication. Solid evidence shows the increase in the hotspot density is responsible for the improvement in the SERS activity of TiO_2-catalyzed Ag NPs. The principle revealed in this study could be used to improve the SERS activity of other NPs or nanostructures.

Acknowledgements

The work is supported by the National Natural Science Foundation of China (Grant Nos. 11364009).

References

[1] S. Nie, S.R. Emory, Probing single molecules and single nanoparticles by surface-enhanced Raman scattering, Science 275 (1997) 1102–1106.
[2] G. Braun, S.J. Lee, M. Dante, T.Q. Nguyen, M. Moskovits, N. Reich, Surface-enhanced Raman spectroscopy for DNA detection by nanoparticle assembly onto smooth metal films, J. Am. Chem. Soc. 129 (2007) 6378–6379.
[3] S. Schlücker, Surface-enhanced Raman spectroscopy: concepts and chemical applications, Angew. Chem. Int. Ed. 53 (2014) 4756–4795.
[4] R.J.C. Brown, M.J.T. Milton, Nanostructures and nanostructured substrates for surface-enhanced Raman scattering (SERS), J. Raman Spectrosc. 39 (2008) 1313–1326.
[5] X.M. Yang, K. Ajito, D.A. Tryk, K. Hashimoto, A. Fujishima, Two-dimensional surface-enhanced Raman imaging of a roughened silver electrode, J. Phys. Chem. 100 (1996) 7293–7297.
[6] R.M. Stöckle, V. Deckert, C. Fokas, R. Zenobi, Controlled formation of isolated silver islands for surface-enhanced Raman scattering, Appl. Spectrosc. 54 (2000) 1577–1583.
[7] Q. Zhou, Y. Liu, Y. He, Z. Zhang, Y. Zhao, The effect of underlayer thin films on the surface-enhanced Raman scattering response of Ag nanorod substrates, Appl. Phys. Lett. 97 (2010) 121902–121904.
[8] N. Félidj, J. Aubard, G. Lévi, J.R. Krenn, A. Hohenau, G. Schider, A. Leitner, F.R. Aussenegg, Optimized surface-enhanced Raman scattering on gold nanoparticle arrays, Appl. Phys. Lett. 82 (2003) 3095–3097.
[9] G. Hong, C. Li, L. Qi, Facile fabrication of two-dimensionally ordered macroporous silver thin films and their application in molecular sensing, Adv. Funct. Mater. 20 (2010) 3774–3783.
[10] X.T. Wang, W.S. Shi, G.W. She, L.X. Mu, S.T. Lee, High-performance surface-enhanced Raman scattering sensors based on Ag nanoparticles-coated Si nanowire arrays for quantitative detection of pesticides, Appl. Phys. Lett. 96 (2010) 053104–053106.
[11] D. Li, L. Pan, S. Wu, S. Li, An active surface enhanced Raman scattering substrate using carbon nanocoils, J. Mater. Res. 28 (2013) 2113–2123.
[12] Q. Tao, S. Li, Q.Y. Zhang, D.W. Kang, J.S. Yang, W.W. Qiu, K. Liu, Controlled growth of ZnO nanorods on textured silicon wafer and the application for highly effective and recyclable SERS substrate by decorating Ag nanoparticles, Mater. Res. Bull. 54 (2014) 6–12.
[13] X. Zhao, B. Zhang, K. Ai, G. Zhang, L. Cao, X. Liu, H. Sun, H. Wang, L. Lu, Monitoring catalytic degradation of dye molecules on silver-coated ZnO nanowire arrays by surface-enhanced Raman spectroscopy, J. Mater. Chem. 31 (2009) 5547–5553.
[14] Q. Gao, A.W. Zhao, Z.B. Gan, W.Y. Tao, D. Li, M.F. Zhang, H.Y. Guo, D.P. Wang, H.H. Sun, R.R. Mao, E.H. Liu, Facile fabrication and growth mechanism of 3D flower- like Fe_3O_4 nanostructures and their application as SERS substrates, CrystEngComm 14 (2012) 4834–4842.
[15] L.M. Sudnik, K.L. Norrod, K.L. Rowlen, SERS-active Ag films from photoreduction of Ag^+ on TiO_2, Appl. Spectrosc. 50 (1996) 422–424.
[16] A. Mills, G. Hill, M. Stewart, D. Graham, W.E. Smith, S. Hodgen, P.J. Halfpenny, K. Faulds, P. Robertson, Characterization of novel Ag on TiO_2 films for surface-enhanced Raman scattering, Appl. Spectrosc. 58 (2004) 922–928.
[17] D. Li, L. Pan, S. Li, K. Liu, S. Wu, W. Peng, Controlled preparation of uniform TiO_2-catalyzed silver nanoparticle films for surface-enhanced Raman scattering, J. Phy. Chem. C 117 (2012) 6861–6871.
[18] K.L. Norrod, L.E. Sudnik, D. Rousell, K.L. Rowlen, Quantitative comparison of five SERS substrates: sensitivity and limit of detection, Appl. Spectrosc. 51 (1997) 994–1001.
[19] S. Li, Q. Tao, D.W. Li, K. Liu, Q.Y. Zhang, Photocatalytic growth and plasmonic properties of Ag nanoparticles on TiO_2 films, J. Mater. Res. 30 (2014) 304–314.
[20] W. Li, P.H.C. Camargo, X. Lu, Y. Xia, Dimers of silver nanospheres: facile synthesis and their use as hot spots for surface-enhanced Raman scattering, Nano Lett. 9 (2009) 485–490.
[21] L. Qin, S. Zou, C. Xue, A. Atkinson, G.C. Schatz, C.A. Mirkin, Designing, fabricating, and imaging Raman hot spots, Proc. Natl. Acad. Sci. 103 (2006) 13300–13303.
[22] S.L. Kleinman, R.R. Frontiera, A.I. Henry, J.A. Dieringer, R.P. Van Duyne, Creating, characterizing, and controlling chemistry with SERS hot spots, Phys. Chem. Chem. Phys. 15 (2013) 21–36.
[23] G. Lu, H. Li, S. Wu, P. Chen, H. Zhang, High-density metallic nanogaps fabricated on solid substrates used for surface enhanced Raman scattering, Nanoscale 4 (2012) 860–863.
[24] S. Li, Study on Photocatalytic Growth of the Ag Nanoparticles Using TiO2 Films and Their SERS Performance, Dalian university of technology, Dalian, 2015, pp. 74–87.
[25] A. Otto, On the significance of Shalaev's 'hot spots' in ensemble and single-molecule SERS by adsorbates on metallic films at the percolation threshold, J. Raman Spectrosc. 37 (2006) 937–947.

[26] Z.Q. Tian, J.S. Gao, X.Q. Li, B. Ren, Q.J. Huang, W.B. Cai, F.M. Liu, B.W. Mao, Can surface Raman spectroscopy be a general technique for surface science and electrochemistry? J. Raman Spectrosc. 29 (1998) 703–711.
[27] P. Hildebrandt, M. Stockburger, Surface-enhanced resonance Raman spectroscopy of rhodamine-6G adsorbed on colloidal silver, J. Phys. Chem. 88 (1984) 5935–5944.
[28] L.C.T. Shoute, A.J. Bergren, A.M. Mahmoud, K.D. Harris, R.L. McCreery, Optical interference effects in the design of substrates for surface-enhanced Raman spectroscopy, Appl. Spectrosc. 63 (2009) 133–140.
[29] Z. Zhang, Z. Zhang, L. Zhang, C. Huang, Electric field enhancements around the nanorod on the base layer, Opt. Exp. 19 (2011) 7274–7279.
[30] J.K. Daniels, G. Chumanov, Nanoparticle-mirror sandwich substrates for surface-enhanced Raman scattering, J. Phy. Chem. B 109 (2005) 17936–17942.